View metadata, citation and similar papers at core.ac.uk
brought to you by CORE
provided by espace@Curtin

Solid/CO_2 and solid/water interfacial tensions as a function of pressure, temperature, salinity and mineral type: Implications for CO_2-wettability and CO_2 geo-storage

Muhammad Arif[1,*], Ahmed Barifcani[1], Stefan Iglauer[1]

[1]Curtin University, Department of Petroleum Engineering, 26 Dick Perry Avenue, 6151 Kensington, Western Australia; phone: +61 8 9266 7703

[*]Corresponding author

Phone: +61 8 9266 7703

Fax: +61 8 9266 7063

Email: muhammad.arif@curtin.edu.au

Abstract:

Wettability of CO_2/brine/mineral systems plays a significant role in the underground geological storage of CO_2 as it governs the fluid flow and distribution mechanism within the porous medium. Technically, wettability is influenced by CO_2 pressure, the temperature of the storage formation, formation water salinity and the type of mineral under investigation. Although a growing number of studies report wettability data for CO_2/water/mineral systems, yet the factors responsible for wettability variation with pressure and temperature remain unclear. In this work, we used the concept of surface energy to explain dependency of wettability on pressure, temperature and salinity. Neumann's equation of state approach was used to compute solid/CO_2 and solid/water interfacial energies using reliable contact angle and CO_2/brine interfacial tension data from the literature at a wide range of operating conditions for quartz, water-wet mica, oil-wet mica and high, medium and low-rank coals. Moreover, the all-important question that why different minerals offer different wettability to CO_2/water systems at the same pressure and temperature of investigation is addressed by comparing the interfacial energies of the minerals. We found that for all minerals solid/CO_2 interfacial energy decreased with pressure and increased with temperature, and solid/water interfacial energy decreased with temperature except for quartz for which solid/water interfacial energy increased with temperature. Furthermore, the solid/CO_2 interfacial energy was lowest for the oil-wet mica

surface and highest for quartz which is due to higher hydrophobicity of oil-wet mica surface. The results of the study lead to a better understanding of the wetting phenomenon at the CO_2/brine/mineral interface and thus contribute towards the better evaluation of geological CO_2-storage processes.

1. Introduction

Carbon capture and storage in depleted hydrocarbon reservoirs or deep saline aquifers contributes significantly towards the reduction of anthropogenic greenhouse gas emissions (Intergovernmental Panel on Climate Change, 2005). CO_2 is also injected into subsurface reservoirs for enhanced oil and gas recovery (e.g. Blunt et al., 1993; Iglauer et al., 2013, 2016; Lackner, 2003). In this context the wettability of CO_2-brine-mineral systems plays a crucial role in deciding the fate of the injected CO_2 within the geological formation (Iglauer et al., 2015a). The existing literature has reported experimental CO_2-wettability data as a function of pressure, temperature and salinity for rock forming minerals such as quartz (Al-Yaseri et al., 2016a; Saraji et al., 2014; Sarmadivaleh et al., 2015), mica (Arif et al., 2016a, b; Broseta et al., 2012; Chiquet et al., 2007) and coals (Arif et al., 2016c; Shojai Kaveh et al., 2012; Siemons et al., 2006). Further, molecular dynamics simulations also computed contact angles for CO_2-brine-quartz systems (Chen et al., 2015; Iglauer et al., 2012; Javanbakht et al., 2015; Liu et al., 2010; McCaughan et al., 2013). However, no significant attention has been given to evaluate the factors which are responsible for wettability variation with pressure, temperature and salinity despite the variations in trends observed in studies on CO_2 wettability of minerals (e.g. θ increased in temperature for quartz/CO_2/brine, Al-Yaseri et al., 2016a and decreased with temperature for mica/CO_2/brine and coal/CO_2/brine systems, Arif et al., 2016a,c).

Recently, a few studies attempted to explain the factors responsible for wettability variation. For instance, Al-Yaseri et al. (2016b) reported that wettability of quartz/gas/brine systems is a strong function of gas density and a mathematical correlation was developed to determine contact angles from gas densities. However, the methodology was applicable to a limited set of operating conditions only. Roshan et al. (2016) developed a physical model based the concept of the diffuse double layer to provide a theoretical framework for changes observed in wettability as a function of pressure, temperature and salinity and found that wettability is strongly related to CO_2/water interfacial tensions and density changes. Ameri et al. (2013) computed sandstone/CO_2 interfacial tension as a function of pressure using Neumann's equation of state (Neumann et al., 1974) and found that the solid/CO_2 interfacial tension

decreased with pressure and they formulated that such change in solid surface energy is responsible for wettability changes. Nevertheless, the factors responsible for wettability variation with pressure, temperature and salinity remain unclear and require further attention.

Theoretically, it is well-established that the contact angle is a function of the interplay of the three interfacial tensions (solid/CO_2, solid/brine and brine/CO_2) as related by Young-Laplace equation below:

$$cos\theta = \frac{\gamma_{sc} - \gamma_{sw}}{\gamma_{cw}} \qquad (1)$$

In equation (1), γ_{sc}, γ_{sw} and γ_{cw} denote solid/CO_2, solid/water and CO_2/water interfacial tensions respectively. To assess the wettability dependence on these interfacial interactions, the quantification of the three interfacial tensions (γ_{sc}, γ_{sw} and γ_{cw}) is essential. In this context, CO_2/water interfacial tensions (γ_{cw}) can be determined experimentally (many studies reported this data e.g. Arif et al., 2016a; Li et al., 2012; Lun et al., 2012), however, an independent experimental measurement of solid/fluid interfacial tension is not possible because a solid interface is very different from a fluid-fluid interface due to absence of mobility (Li and Neumann, 1992). Consequently, the use of numerical/empirical techniques such as Neumann's equation of state becomes essential (Neumann et al., 1974). They applied this method to compute surface energies of low energy polymers (Neumann et al., 1974, Kwok and Neumann, 1999). We, thus, extend the use of Neumann's equation of state to compute mineral/CO_2 and mineral/water interfacial tensions as a function of pressure, temperature, salinity and mineral type. Essentially, three important issues are addressed in this work: 1) Computation of surface energy of solid/CO_2 and solid/brine as a function of pressure, temperature and salinity, 2) How these computed interfacial tensions explain the dependence of wettability on pressure, temperature and salinity and 3) To answer a very important question, i.e. why different minerals exhibit different wettability at the same operating conditions.

In this context, we used advancing and receding contact angle (θ_a and θ_r respectively) data for CO_2/brine systems for quartz (from Al-Yaseri et al., 2016a), water-wet mica (from Arif et al., 2016a; and the mica chosen is muscovite mica), oil-wet mica (from Arif et al., 2016b) and coal (from Arif et al., 2016c) at a wide range of operating conditions and computed mineral/CO_2 and mineral/water interfacial tensions and analysed the associated trends. Our results depict that mineral/CO_2 interfacial tension decreased with pressure and increased with temperature for all minerals. However, mineral/water interfacial tension decreased with temperature for mica and coals but increased with temperature for quartz. The computed data in this paper can also be used to estimate contact angle from Young's equation at any pressure, temperature and

salinity using known values of surface energies. Finally, we conclude that the quantification of surface energies is not only helpful in understanding the CO_2/solid interactions but also adequately explain the factors influencing wettability and thus considerably improve the understanding of geological storage processes and provide independent estimates for surface energies for various other engineering applications.

2. Methodology

We used the equation of state approach by Neumann (Neumann et al., 1974) to compute mineral/CO_2 and mineral/water surface energies for a wide range of operating conditions for quartz, water-wet mica, oil-wet mica, and coals of high, medium and low ranks. Following sections describe the methodology in detail.

2.1. Contact angle data

We selected the water advancing and receding contact angle (θ_a and θ_r) data from our previous publications (quartz: from Al-Yaseri et al., 2016a, water-wet mica from Arif et al., 2016a, and oil-wet mica from Arif et al., 2016b; high, medium and low rank coals: from Arif et al., 2016c; Table 1). Surface energy calculations require equilibrium contact angles (see detail in section 2.2 below); these have been computed from Tadmor's empirical method (Tadmor, 2004, Table 2). Tadmor's correlation allows the calculation of equilibrium contact angles using the corresponding values of advancing and receding contact angles. The equations are as follows:

$$\theta_e = arccos\left(\frac{\Gamma_A \cos\theta_A + \Gamma_R \cos\theta_R}{\Gamma_A + \Gamma_R}\right) \quad (2)$$

In equation (2), θ_e is the equilibrium contact angle while θ_A and θ_R are the advancing and receding contact angles respectively, whereas, Γ_R and Γ_A are defined as follows:

$$\Gamma_R = \left(\frac{\sin^3\theta_R}{2 - 3\cos\theta_R + \cos^3\theta_R}\right)^{1/3} \quad (3)$$

$$\Gamma_A = \left(\frac{\sin^3\theta_A}{2 - 3\cos\theta_A + \cos^3\theta_A}\right)^{1/3} \quad (4)$$

Neumann et al.'s equation of state approach also requires CO_2/water interfacial tension data which was taken from Sarmadivaleh et al. (2015) and CO_2/brine interfacial tension was taken from Arif et al. (2016a), Table 3.

Table 1: Contact angle data for CO_2-deionized (DI) water systems for minerals investigated in this study.

Temperature (K)	Pressure (MPa)	Quartz		Water-wet mica		Oil-wet mica		High rank coal		Medium rank coal		Low rank coal	
		θ_a (°)	θ_r (°)	θ_a (°)	θ_r (°)	θ_a (°)	θ_r (°)	θ_a (°)	θ_r (°)	θ_a (°)	θ_r (°)	θ_a (°)	θ_r (°)
308*	0.1	0	0	10	5	90	65	37	30	32	25	43	32
	5	15	11	33	25	125	107	94	80	77	63	75	60
	10	23	17	55	50	148	128	140	126	127	115	103	87
	15	30	20	71	63	170	159	146	134	128	118	112	96
	20	37	23	80	72	172	160	151	139	137	121	122	110
323	0.1	0	0	4	0	74	64	51	45	28	22	38	27
	5	19	13	30	24	118	102	89	79	69	49	50	42
	10	30	25	48	40	143	125	129	114	108	98	94	78
	15	38	28	59	54	170	157	136	123	114	102	102	91
	20	42	35	70	62	170	158	141	129	122	112	116	107
343	0.1	0	0	0	0	73	65	58	53	18	12	27	18
	5	22	19	27	22	99	82	86	74	48	33	45	36
	10	42	30	43	36	108	91	109	97	95	85	92	77
	15	45	38	52	48	128	110	119	111	102	89	102	87
	20	50	42	62	53	156	134	125	114	113	95	110	97

*contact angles are interpolated at 308 K for quartz

Table 2: Equilibrium contact angles for all minerals calculated using Tadmor's correlation.

Temperature (K)	Pressure (MPa)	Equilibrium contact angle θ_e (°)					
		Quartz	Water-wet mica	Oil-wet mica	High rank coal	Medium rank coal	Low rank coal
308	0.1	0	6	74.1	33.3	28.2	36.9
	5	12.9	28.7	112.8	85.8	69	66.4
	10	19.8	52.4	131.8	130	119	93.2

	15	24.2	66.7	159.9	137	122	102
	20	29	75.7	160.5	142	126	115
323	0.1	0	2	68.49	47.8	24.8	31.9
	5	15.7	26.8	107.7	83.4	57.1	45.7
	10	27.4	43.7	129.3	119	102	84.4
	15	32.5	56.4	157.8	127	107	95.6
	20	38.3	65.7	158.8	133	116	111
343	0.1	0	0.5	68.67	55.4	14.7	22
	5	20.4	24.3	88.62	79.2	39.4	40.1
	10	35.3	39.3	97.35	102	89.3	83.1
	15	41.3	49.9	115.6	114	94.3	92.9
	20	45.7	57.1	136.6	118	101	102

Table 3: CO_2/DI-water and CO_2/brine interfacial tension data used.

Temperature (K)	Pressure (MPa)	CO_2/DI-water IFT[a] (mN/m)	CO_2/brine* IFT[b] (mN/m)
308	0.1	75.8	72.9
	5	40.2	50.1
	10	28.4	38.2
	15	22.7	33.9
	20	21.0	32.3
323	0.1	73.1	72.0
	5	49	55.3
	10	35.5	42.6
	15	29	38.7
	20	26	36.0
343	0.1	65	69.2
	5	52.18	57.7
	10	43	44.8
	15	34.5	39.7
	20	27	37.7

[a] experimental data from Sarmadivaleh et al. (2015), values interpolated at 308 K and 323 K

[b] experimental data from Arif et al. (2016a)

149 *20wt% NaCl in DI water

150

151

152

153

154 **2.2. Surface free energy computation**

155 The surface free energy of solids has been investigated by a growing number of studies (e.g.
156 Ameri et al., 2013; Dickson et al., 2006; Kwok and Neumann, 2000; Zenkiewicz, 2007) as it
157 is of great practical significance for many engineering applications including catalysis,
158 coatings, flotation, printing and polymer sciences (Zenkiewicz, 2007). The most common
159 approaches include the Zisman method (Fox and Zisman, 1952), the Fowkes method (Fowkes,
160 1964), the geometric-mean approach (Owens and Wendt, 1969), the harmonic-mean approach
161 (Wu, 1971), the equation of state approach or Neumann's method (Neumann et al., 1974) and
162 the acid-base approach or van Oss-Good method (van Oss et al., 1986). We chose Neumann's
163 equation of state method because of convenience in its application as it requires the knowledge
164 of experimental contact angle, θ, and CO_2/water interfacial tension (γ_{cw}) data for which reliable
165 data is available.

166

167 Thermodynamically, solid/CO_2, solid/water and CO_2/water interfacial tensions (γ_{sc}, γ_{sw}
168 and γ_{cw}) are interrelated by an equation of state (Neumann et al., 1974), such that:

169

170 $$\gamma_{SW} = f(\gamma_{SC}, \gamma_{CW}) \quad (5)$$

171

172 Neumann et al. (1974) used the hypothesis that the free energy of adhesion per unit area of a
173 solid-liquid pair is equal to the work required to separate a unit area of solid-liquid interface
174 and that free adhesion energy was proposed to be equal to the geometric mean of the solid
175 cohesion work and the liquid cohesion work. These geometric means were combined so that
176 equation (6) resulted (for a complete derivation the reader is referred to Ameri et al., 2013).

177

178 $$\gamma_{sw} = \gamma_{sc} + \gamma_{cw} - 2\sqrt{\gamma_{cw}\gamma_{sc}}[1 - \beta(\gamma_{cw} - \gamma_{sc})^2] \quad (6)$$

179

180 The equation (7) below was then derived by Ameri et al., (2013) to find an expression for γ_{sc}
181 instead of γ_{sw} as shown:

$$\gamma_{sc} = \gamma_{sw} + \gamma_{cw} - 2\sqrt{\gamma_{cw}\gamma_{sw}}[1 - \beta(\gamma_{cw} - \gamma_{sw})^2] \quad (7)$$

'β' is a constant which is related to the fit of the original experimental data (Neumann et al., 1974) to the model and in the present case it can be determined by non-linear regression of contact angle (θ) and CO_2/water interfacial tension data (γ_{cw}) as further explained below.

Combining Eq. (1) and (7), one obtains:

$$\cos\theta_e = 1 - 2\sqrt{\frac{\gamma_{sw}}{\gamma_{cw}}}[1 - \beta(\gamma_{cw} - \gamma_{sw})^2] \quad (8)$$

Ameri et al., (2013) applied equation (7) and (8) to determine solid/CO_2 interfacial tension of oil-wet Bentheimer sandstone as a function of pressure and they reported the corresponding values of solid/liquid interfacial tension derived by non-linear regression. To account for a systematic evaluation of wettability dependence on pressure, temperature and salinity, we express equations (7) and (8) to clearly demonstrate that these are functions of pressure, temperature and salinity:

$$\gamma_{sc(P,T,S)} = \gamma_{sw(T,S)} + \gamma_{cw(P,T,S)} - 2\sqrt{\gamma_{cw(P,T,S)}\gamma_{sw(T,S)}}\left[1 - \beta\left(\gamma_{cw(P,T,S)} - \gamma_{sw(T,S)}\right)^2\right] \quad (9)$$

$$\cos\theta_{e_{(P,T,S)}} = 1 - 2\sqrt{\frac{\gamma_{sw(T,S)}}{\gamma_{cw(P,T,S)}}}\left[1 - \beta\left(\gamma_{cw(P,T,S)} - \gamma_{sw(T,S)}\right)^2\right] \quad (10)$$

The scripts P, T and S refer to pressure, temperature and salinity, respectively, and are added to the interfacial energy terms to elucidate their dependence on them. It is notable that γ_{sw} is dependent on temperature and salinity but not on pressure (Ameri et al., 2013; Neumann et al., 1974). This is the basic assumption of the Neumann's equation of state.

Our computations begin with input data acquisition which includes a) advancing and receding contact angle data for quartz (Al-Yaseri et al., 2016a), water-wet mica (Arif et al., 2016a), oil-wet mica (Arif et al., 2016b) and coals of high medium and low ranks (Arif et al., 2016c) listed in Table 1, and b) CO_2/water interfacial data (Sarmadivaleh et al., 2015), listed in Table 3. Then, $\cos\theta_e$ (cosine of the equilibrium contact angle) is calculated using advancing and receding contact angle data for all cases analysed (results in Table 2). In the next step, $\gamma_{sw(T)}$ and the constant 'β' are determined by least squares fitting of the $\cos\theta_e$ and γ_{cw} data. To accomplish this, $\cos\theta_e$ is first calculated by using equation (10) for any trial values of $\gamma_{sw(T)}$ and 'β' and is plotted against γ_{cw} (this data is referred as model data). Moreover, the experimental $\cos\theta_e$ (Table 2) is also plotted against γ_{cw} (such a plot is shown in Figure 1 for all minerals analysed at 343 K), the regression analysis of these data-sets yield final values of $\gamma_{sw(T)}$ and 'β' corresponding to the best-fit (note: such plots are created at all three analysis temperatures and for all minerals, and directly provide values of $\gamma_{sw(T)}$ as a function of temperature). Finally, using these calculated values, solid/CO_2 interfacial tension is computed using equation (9) as a function of pressure, temperature, salinity and type of the mineral.

2.3. Regression fit of data

As a first step, $\cos\theta_e$ (experimental) is plotted against γ_{cw} and on the same plot $\cos\theta_e$ (calculated using equation 10 for arbitrary values of γ_{sw} and 'β') is also plotted against γ_{cw}. Such plots are constructed corresponding for each temperature and for all five cases analysed. An example is shown in Figure 1, where, for simplicity, only a temperature of 343 K is shown, but for all five minerals investigated. The model and experimental data are in a good agreement, however the model predictions are sensitive to CO_2/water interfacial tension values and thus reliable CO_2/interfacial tension input is required for reliable modelling of solid/fluid interfacial tensions.

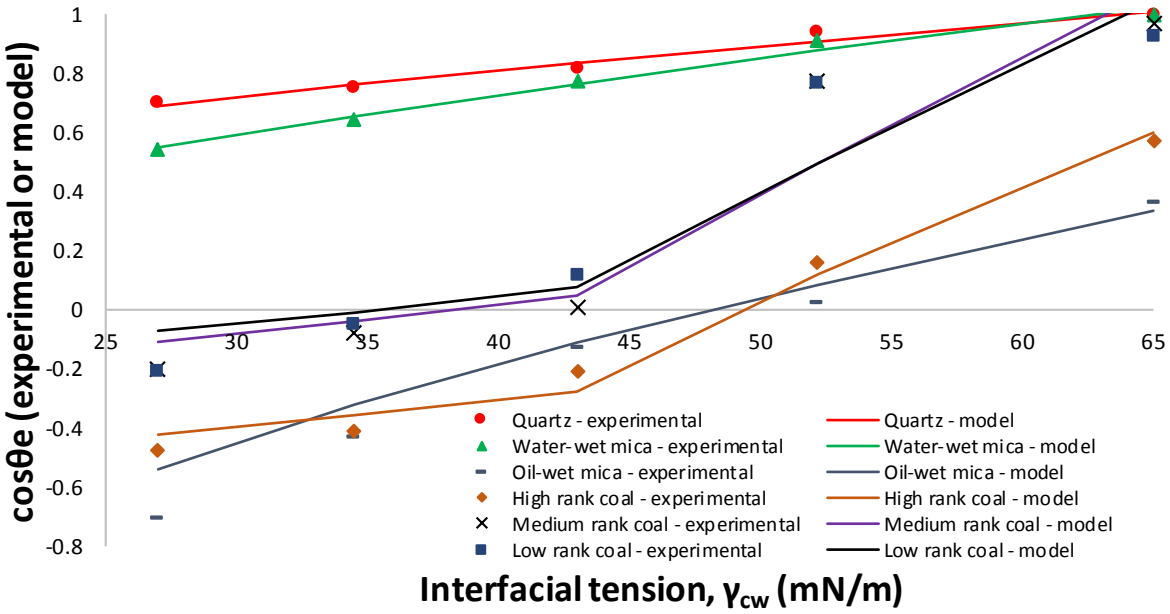

Figure 1: Regression fit of experimental and model data for all minerals investigated at 343 K.

The R^2-values, fitting parameters 'β' and γ_{sw} were computed for each case from the regression fits and the results are tabulated in Table 4. The standard deviations in experimental contact angle and interfacial tension data used were ±3° and ±3 mN/m respectively.

Table 4: Results obtained from regression fit of the experimental and model data.

Case	Temperature (K)	R^2	β	γ_{sw} (mN/m)
Quartz	308	0.898	0.000205	0.058
	323	0.943	0.000219	0.284
	343	0.988	0.0002524	0.952
Water-wet mica	308	0.899	0.00022	2.178
	323	0.935	0.00023	2.048
	343	0.992	0.00027	1.98
Oil-wet mica	308	0.9857	0.000166	20.19
	323	0.988	0.00022	25.47
	343	0.92	0.000145	16.53
High rank coal	308	0.9778	0.00033	20.25
	323	0.952	0.00028	19.23

	343	0.944	0.00021	15.37
Medium rank coal	308	0.994	0.00031	16.17
	323	0.974	0.0003	13.87
	343	0.93	0.00034	10.81
Low rank coal	308	0.989	0.00022	11.22
	323	0.954	0.0003	10.38
	343	0.946	0.00032	10.12

242
243
244
245

246 3. Results and discussion

247

248 We computed solid/CO_2 interfacial tension as a function of pressure, temperature and salinity
249 and solid/water interfacial tension as a function of temperature and salinity via Neumann's
250 equation of state (Neumann et al., 1974) for quartz, mica and coals using experimental contact
251 angle data and CO_2/brine interfacial tension data. The results broaden the understanding of
252 rock/fluid interaction properties. Specifically, the results of this study allow the understanding
253 of the influence of surface energy on rock wettability as a function of pressure, temperature,
254 salinity, and type of mineral. Thus, the results contribute to a better understanding of storage
255 mechanisms which ensure containment security (Iglauer et al., 2015b; Krevor et al., 2012;
256 Krevor et al., 2015).

257
258

259 3.1. Effect of pressure on solid/CO_2 interfacial tension

260

261 *3.1.1 Case 1: quartz*

262 γ_{sc} (solid/CO_2 interfacial tension) decreased with pressure at all temperatures and for all cases
263 analysed (Figure 2-4). As the pressure increased from 0.1 MPa to 10 MPa, quartz/CO_2
264 interfacial tension decreased sharply from 75 mN/m to 31 mN/m at 323 K (Figure 2). However,
265 the decrease flattened for an additional pressure increment (from 15 MPa to 20 MPa it changed
266 from 24.6 mN/m to 21.6 mN/m, a reduction of only 3 mN/m). A similar trend was found at
267 elevated temperature, 343 K. Physically, as the pressure increases, the cohesive energy density
268 of CO_2 increases and approaches to the cohesive energy of the substrate (Dickson et al., 2006).

Eventually, the interactions between solid and CO_2 become more favourable and as a result quartz/CO_2 interfacial energy decreases with pressure. Note that at pressure = 0.1 MPa, a switch in temperature occurs due to a switch in CO_2/water interfacial tensions; Table 3 (Arif et al., 2016a).

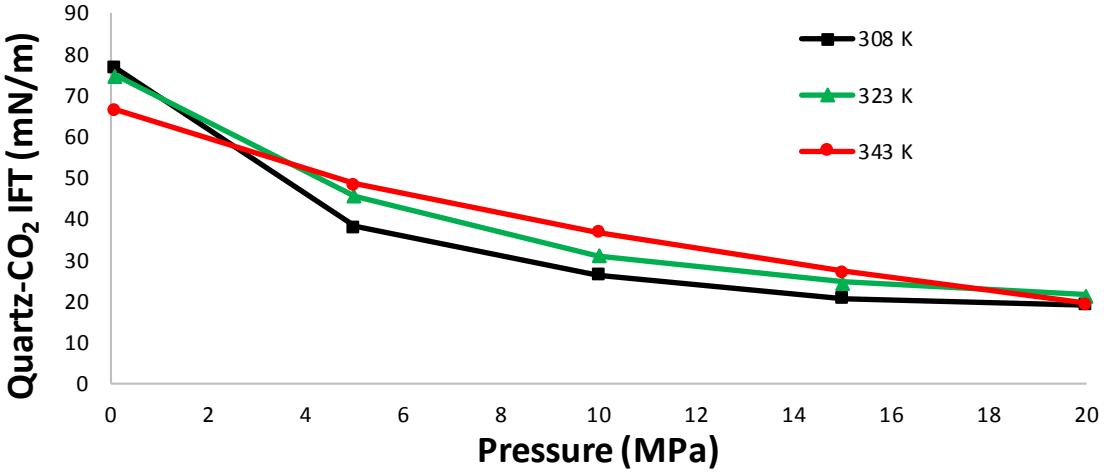

Figure 2: Quartz/CO_2 interfacial tension as a function of pressure and temperature.

A few studies report surface free energies of quartz at ambient conditions. Janczuk and Zdziennicka, (1994) calculated the surface energy of quartz at ambient conditions against air using the van Oss-Good method (van Oss et al., 1986) and the values ranged from 57 mN/m to 126 mN/m, consistent with our value (~74 mN/m) estimated for a similar condition (0.1 MPa and 308 K).

Dickson et al. (2006) is the only major study which computed surface energies as a function of pressure for silica (glass)/CO_2 systems and found that for a partially methylated glass surface (63% of the surface was covered by methyl groups, the remaining 37% by SiOH groups) surface solid/CO_2 interfacial tension decreased with pressure. The values reported were 38 mN/m at a CO_2 activity of 0 (equivalent to a pressure of 0.1 MPa) and reduced to ~10 mN/m at a CO_2 activity of 1.4 (equivalent to 20 MPa) at 296 K. The decrease in quartz/CO_2 interfacial tension with pressure is thus consistent with Dickson et al. (2006), however, the difference in values is due to the fact that the surface they used had only 37% silanol group coverage (while in our case it is 100%, i.e. pure quartz). Furthermore, Dickson et al. (2006) reported solid/CO_2 interfacial tension for a 12% SiOH surface (now 88% of the surface was methylated), for which lower γ_{sc} values were reported (20 mN/m at 0.1 MPa and ~0 mN/m at 20 MPa) which is due to

294 the higher hydrophobicity of the 12% SiOH surface (when compared with the 37% SiOH
295 surface). Due to the limited number of silanol groups available, only a minimal amount of CO_2
296 is expected to cap these hydrophilic sites, thus γ_{sc} values were lower for lower silanol coverage
297 (e.g. for our case γ_{sc} = 20 mN/m at 20 MPa, and for Dickson et al. γ_{sc} = 10 mN/m for 37% SiOH
298 surface, and ~0 mN/m for 12% SiOH surface).
299 The higher values of quartz/CO_2 interfacial tensions as compared to mica (see below) at a given
300 pressure and temperature imply that quartz is more hydrophobic in nature.
301
302 *3.1.2 Case 2: Mica*
303 Two mica surfaces were analysed: a) naturally water-wet mica (Arif et al., 2016a) and b) oil-
304 wet mica (treated with silane to achieve oil-wet conditions, ambient air/water contact angle =
305 120°, Arif et al., 2016b). The results indicate that, likewise quartz, mica/CO_2 interfacial tension
306 decreased with pressure for both water-wet and oil-wet mica surfaces (Figure 3). When
307 pressure increased from 0.1 MPa to 5 MPa, mica/CO_2 interfacial tension decreased sharply
308 from 78 mN/m to 41 mN/m, for water-mica. Gradually, the decrease flattened out with further
309 increase in pressure (24 mN/m at 10 MPa and 16 mN/m at 20 MPa). Similar trends were found
310 for oil-wet mica surface. However, at any given pressure, the mica/CO_2 interfacial tension was
311 considerably higher for water-wet mica. For example, at 10 MPa and 343 K, mica/CO_2
312 interfacial tension was 40 mN/m for water-wet mica and only 4.6 mN/m for oil-wet mica
313 surface. This result is quite remarkable – as it demonstrates that the hydrophobic surfaces (e.g.
314 oil-wet mica - higher water contact angles) have considerably lower solid/CO_2 interfacial
315 energies in comparison to the hydrophilic surfaces (e.g. water-wet mica, lower water contact
316 angles, and quartz, even lower contact angles than water-wet mica). The permanent oil coating
317 on the mica (to be precise: the C12 alkyl rests chemically bonded to the surface) is responsible
318 for the low surface energy of the oil-wet mica surface. Moreover, it can also be established that
319 the higher the solid/vapour surface energy, the higher is the tendency of the surface to wet with
320 water (i.e. lower contact angles, e.g. Table 1). The results are consistent with Ameri et al.
321 (2013) who used a similar methodology and computed interfacial interaction of CO_2 and oil-
322 wet Bentheimer. Their results show that at any pressure, solid/CO_2 interfacial tension was
323 lower for the more oil-wet cores. For instance, at 10 MPa and 318 K, solid/CO_2 interfacial
324 tensions were 20 mN/m for relatively more water-wet Bentheimer (SB-1) and 1 mN/m for oil-
325 wet Bentheimer (SB-6, Ameri et al. 2013).
326 These results are significant for understanding the fluid flow dynamics in oil-wet and water-
327 wet reservoir and caprocks (Iglauer et al. 2015a), and also for material design and development

where the physicochemical surface characteristics (e.g. surface energy) play a key role for a wide range of operating conditions (Zenkiewicz, 2007).

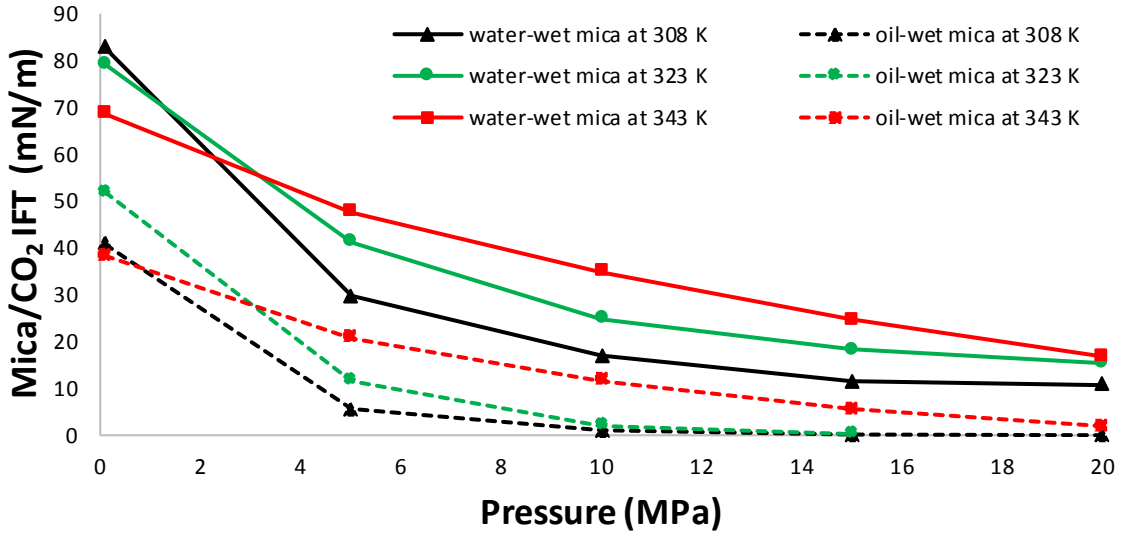

Figure 3: Mica/CO_2 interfacial tension as function of pressure and temperature.

3.1.3 Case 3: Coals

Three coal samples [high rank (semi anthracite; from Hazelton, Pennsylvania, USA), medium rank (medium volatile bituminous; from Morgantown, West Virginia, USA), and low rank (lignite; from North Dakota, USA] were analysed for surface energy calculations. Advancing and receding contact angle data for the three coals is taken from our previous work (Arif et al., 2016c, Table 1). The detailed description of the properties of these coal sample can be found elsewhere (Arif et al., 2016c), however the mineral identified by XRD in the three samples revealed that the major minerals present were illite, quartz and kaolinite. We note that the measured contact angles may slightly vary with the minerology of coal; thus the results reported here must be accompanied with the minerology of the specific sample under investigation. Results showed that coal/CO_2 interfacial tension also decreased with pressure irrespective of the coal rank (Figure 4). For all coals, the coal/CO_2 interfacial tension decreased sharply for the pressure interval 0.1 MPa-5 MPa, e.g. for high rank coal, at 308 K, coal/CO_2 interfacial tension decreased from 84 mN/m to ~12 mN/m when pressure increased from 0.1 MPa to 5 MPa. However, γ_{sc} turned almost constant for the pressure interval 10 MPa – 20 MPa (Figure 4). Moreover, at a given pressure, the low rank coals exhibited the highest coal/CO_2

interfacial tension values, while the high rank coal had the lowest coal/CO_2 interfacial tension, e.g. at 10 MPa and 323 K, coal/CO_2 interfacial tensions were 4.7 mN/m, 7.4 mN/m, and 10.2 mN/m for high, medium and low rank coals, respectively. At ambient conditions, Staszczuk (1989) determined surface free energy of coal, and found that the dispersion component was 45 mN/m and polar component measured 13 mN/m, thus a total surface energy of 58 mN/m comparable to our results ~ 70 mN/m for low rank coal at 308 K and 0.1 MPa.

In order to explain the variation of coal/CO_2 interfacial tension with coal rank, we conducted FTIR (Fourier Transformed infrared) spectroscopy measurements on the coal samples (Figure 5). Low rank coal demonstrated the largest peak beginning at about 2800 cm^{-1} and ending at 3800 cm^{-1} which is attributed to the O-H and N-H stretch vibrations (Socrates, 2004) while high rank coal exhibited negligible O-H and N-H stretch vibrations at 3800 cm^{-1}. The abundance of these hydrophilic sites in low rank coal and absence of these sites in high rank coal is responsible for higher coal/CO_2 interfacial tensions for low rank coal and low coal/CO_2 interfacial tension for high rank coal. The band at ~2900 cm^{-1} observed for low and medium rank coal is due to the presence of aliphatic C-H stretching vibrations (Wu et al., 2014); however, its absence in high rank coal is unusual and is perhaps due to C-H stretching where the carbon is in a C=C bond. The rough part of the spectra for 2000-2400 cm^{-1} should be ignored as this is where the ATR crystal is absorbing itself (diamond) and the bands don't always perfectly cancel out.

Moreover, the sharp band observed at 1500-1800 cm^{-1} for low and medium rank coal is attributed to aromatic ring vibrations, which are enhanced by oxygen groups (Sarwar et al., 2012). The corresponding shoulder peaks at 1600 cm^{-1} for low and medium rank coals is attributed to C=O stretching vibrations and these represent all C=O functionalities, e.g. carboxylic acids or phenolic esters (Manoj et al., 2009). Furthermore, low and medium rank coal (medium volatile bituminous) exhibited significantly stronger bands (in comparison to high rank coal) at wave numbers from 600-800 cm^{-1} and 1000-1100 cm^{-1} indicating presence of more C-S stretching vibrations and C-H out of plane bending.

Thus, low rank coal has more polar functional groups on the surface than medium rank coal, and thus fewer attractive forces between the more polar surface and the non-polar (here in the sense of no external dipole moment) CO_2 generated, which lead to the higher coal/CO_2 interfacial tension for low rank coal at any pressure as compared to medium and high rank coals (Figure 4).

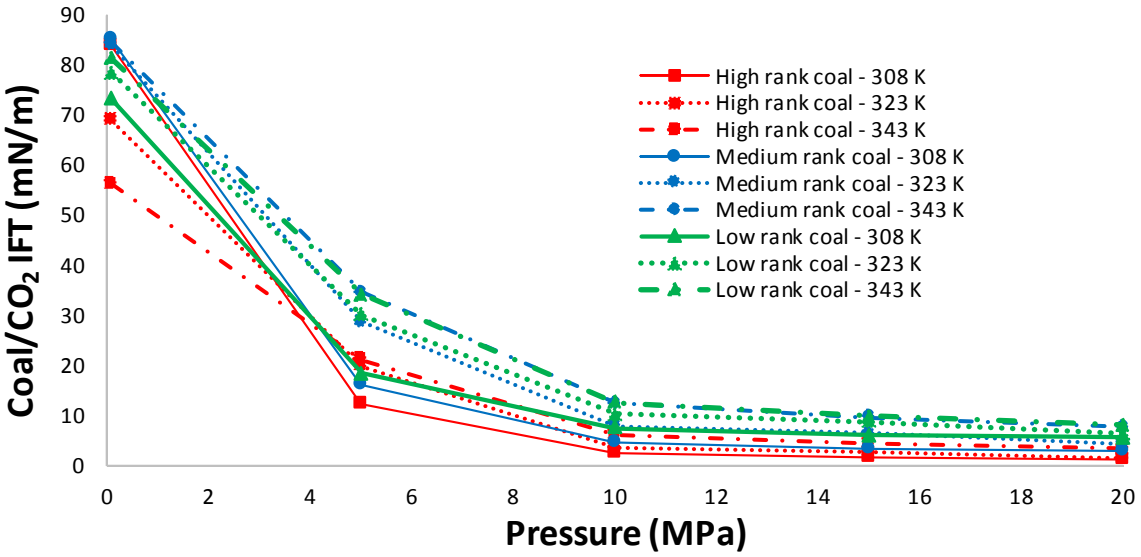

Figure 4: Coal/CO_2 interfacial tension as a function of pressure, temperature and coal rank.

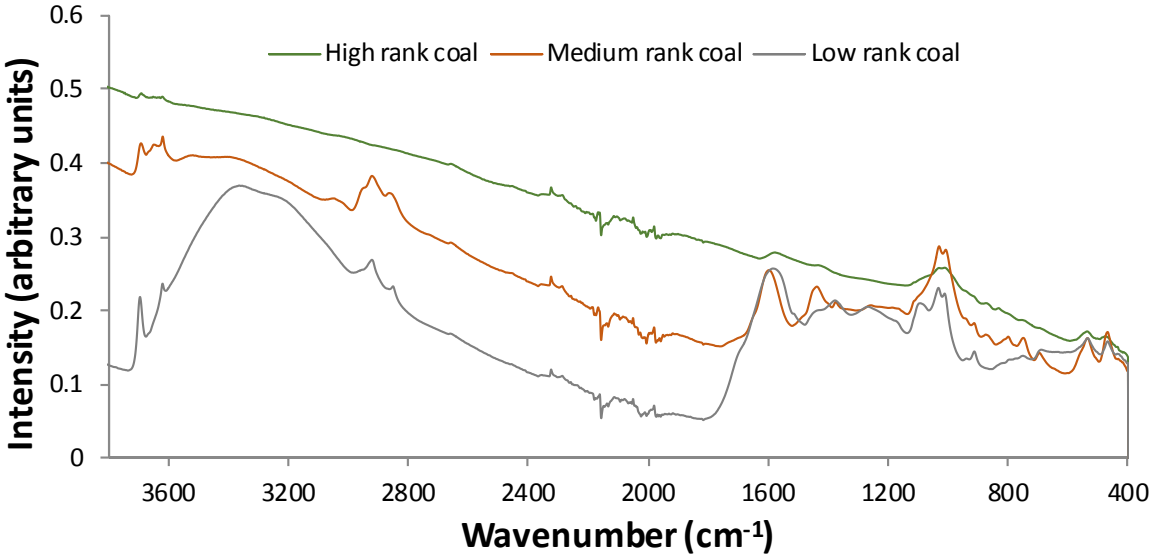

Figure 5. ATR-Infrared spectra for low, medium and high rank coals.

Note that high surface energy corresponds to strong cohesive forces and higher boiling points (Tripp and Combes, 1998). Moreover, high energy surfaces tend to reduce energy by adsorption of contaminants from the environment (Tripp and Combes, 1998).

3.2. Effect of temperature on solid/CO_2 interfacial tension

For all cases analysed, the solid/CO_2 interfacial tension increased with temperature (Figures 2-4). For simplicity, a plot of solid/CO_2 interfacial tensions for the temperature range 308-343 K at 15 MPa is presented in Figure 6.

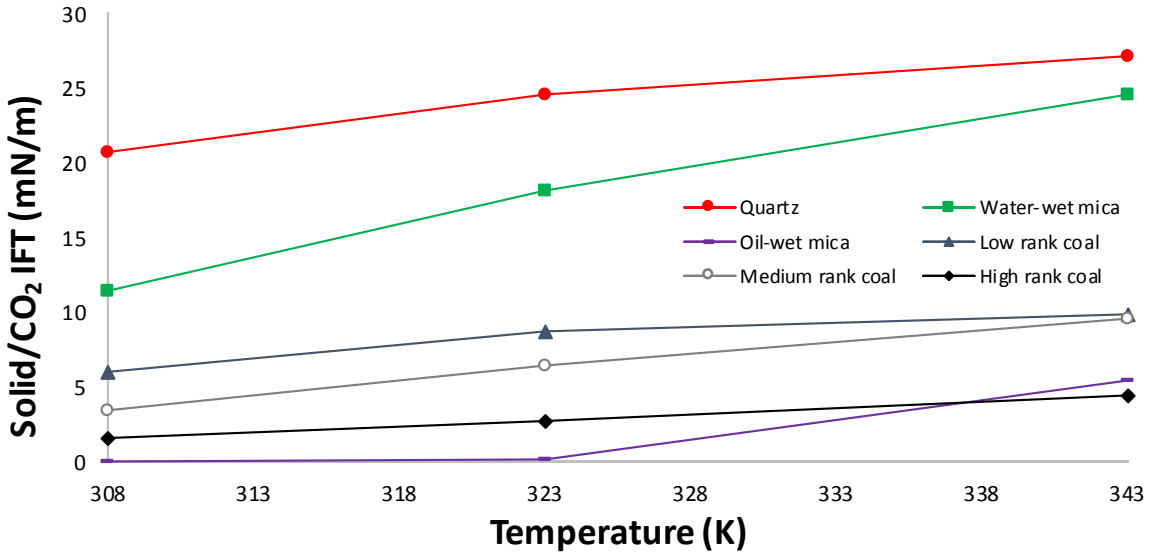

Figure 6: Solid/CO_2 interfacial tension as a function of temperature at 15 MPa for various substrates.

Quartz/CO_2 interfacial tension increased from 21 mN/m to 27 mN/m when temperature increased from 308 K to 343 K (Figure 6). Moreover, solid/CO_2 interfacial tension was highest for quartz, and lowest for oil-wet mica at any pressure and temperature.

Mica/CO_2 interfacial tension also followed a similar trend. For water-wet mica, mica/CO_2 interfacial tension increased from 11.5 mN/m to 24 mN/m when temperature increased from 308 K to 343 K, while for the same temperature interval, for oil-wet mica, mica/CO_2 interfacial tension increased from ~ 0 mN/m to 5 mN/m. Moreover, oil-wet mica demonstrated the lowest values of mica/CO_2 interfacial tension out of all cases at any pressure and temperature which is again attributed to reduced number of polar sites on oil-wet mica surface.

Coal/CO_2 interfacial tension also decreased with temperature, (Figure 6). For instance, for low rank coal, coal/CO_2 interfacial tension increased from 6 mN/m to ~ 9.5 mN/m when temperature increased from 308 K to 343 K. Moreover, high rank coal had the lowest coal/CO_2 interfacial tension at any temperature which is due to the lower concentration of polar surface

groups on the high rank coal (see above and Figure 5). Moreover, we point out that higher coal/CO_2 interfacial tensions reduces CO_2-adsorption in coals (because CO_2-adsorption in coals also decreases with temperature, Bustin and Clarkson, 1998).

For all cases analysed, the increase in γ_{sc} with temperature is attributed to a decrease in cohesive energy density of CO_2 with temperature (Barton, 1991) while the cohesive energy density of the solid is expected to stay approximately constant with temperature (Kittel, 2005), which leads to an increase in the difference of solid/CO_2 cohesive energies with temperature. Consequently, the interactions between solid and CO_2 become less favourable, thus γ_{sc} increases with temperature which promotes water-wetting of the surface. Moreover, reduction in CO_2 density with temperature leads to fewer van der Waals interactions which leads to an increase in γ_{sc} with temperature.

3.3. Effect of temperature on solid/water interfacial tension

Solid/water interfacial tension is directly computed from the regression fit of the experimental and model data and the results are shown in Table 4. For all cases, the solid/water interfacial tension decreased with increasing temperature except for quartz, for which it increased with temperature. However, the absolute quartz γ_{sw} was very low and so were the changes in γ_{sw}. When temperature increased from 308 K-343 K the quartz/water interfacial tension increased from 0.058 mN/m to 0.952 mN/m. Recently, Shojai Kaveh et al. (2016) calculated interfacial energy of shale/water systems and found that the values of shale/water interfacial tension was also quite low (0.58 mN/m at 318 K), consistent with our results. The increase in quartz/water interfacial tension with temperature is due to desorption of water molecules from the surface (Janczuk and Zdziennicka, 1994).

For mica, at any temperature, the solid/water interfacial tensions were notably higher for oil-wet mica and lower for water-wet mica (e.g. γ_{sw} = ~ 25 mN/m for oil-wet mica (21% carbon coverage, Arif et al., 2016b), and ~2 mN/m for water-wet mica (0% carbon coverage, unaltered surface, Arif et al., 2016b) at the same temperature, 323 K and pressure, 10 MPa). The larger solid/liquid interfacial tension values for the more hydrophobic surface is consistent with Dickson et al. (2006) who reported that the glass surface with higher silanol coverage had lower solid/liquid interfacial tensions (note: a higher concentration of surface silanol groups creates a more hydrophilic surface (Chen et al., 2015; McCaughan et al., 2013). Specifically, the calculated γ_{sw} values for the 37% SiOH and 12% SiOH surfaces were 13.2 and 29.2 mN/m

456 respectively (Dickson et al., 2006), quite comparable to our results for the oil-wet mica
457 surfaces. The results are also consistent with Ameri et al. (2013) who reported that γ_{sw} was
458 significantly lower for water-wet sandstones (γ_{sw} = 2.88 mN/m) as compared to oil-wet
459 sandstones (γ_{sw} = 27.22 mN/m).
460 Coal surfaces also exhibited similar trends, i.e. γ_{sw} decreased with increasing temperature, and
461 the values of coal/water interfacial tension were higher for high rank coal and lower for low
462 rank coal (e.g. at 323 K, γ_{sw} was 19.23 mN/m for high rank coal, 13.87 mN/m for medium
463 rank coal and 10.38 mN/m for low rank coals, Table 4). This effect is attributed to an abundance
464 of hydrophilic sites (OH functional groups, typically silanol) in low rank coal and absence of
465 hydrophilic sites in high rank coal. Essentially, presence of silanol sites leads to favourable
466 interactions between coal surface and water, thereby resulting in a reduction of γ_{sw} for low
467 rank coal.
468 Further, we point out that the proposed methodology assumes that γ_{sw} is constant versus
469 pressure. In reality, however, the solid/water interactions are expected to change due to increase
470 in solubility of CO_2 in water with pressure (El-Maghraby et al. 2012), and associated lower pH
471 values (Schaeff and McGrail, 2004), which leads to increased protonation of the silanol surface
472 groups (Brown et al., 2012).
473
474 *3.4. Effect of salinity on solid/CO_2 interfacial tension*
475
476 We compared solid/CO_2 interfacial tension (as function of pressure and temperature) for 20
477 wt% NaCl brine in mica/CO_2 systems and compared it with that of mica/water systems. The
478 results showed that the mica/CO_2 interfacial tension for DI-water at a particular pressure and
479 temperature is quite similar to the mica/CO_2 interfacial tension for 20 wt % NaCl brine case
480 (Figure 7). For instance, at 323 K, and 10 MPa, the mica/CO_2 interfacial tensions were 22.4
481 mN/m for liquid comprising of 20 wt% NaCl brine, and 24.8 mN/m for DI-water, thus a
482 difference of only 2.4 mN/m (Figure 7). Moreover, at the same temperature but at 15 MPa,
483 mica/CO_2 interfacial tension for two different liquids (DI water and 20 wt % NaCl brine) is the
484 same (~18.5 mN/m, Figure 7). In summary, the R^2-values for the correlation between mica/CO_2
485 interfacial tensions for the two liquids were 0.997, 0.998 and 0.985 at 308 K, 323 K and 343
486 K, respectively, indicating a strong correlation. This implies that solid/CO_2 interfacial tension
487 is not much changed by altering the type of the liquid in the same system. We point out that

this result verifies this methodology and our predictions (of mineral/CO_2 and mineral/water interfacial tensions) to some extent.

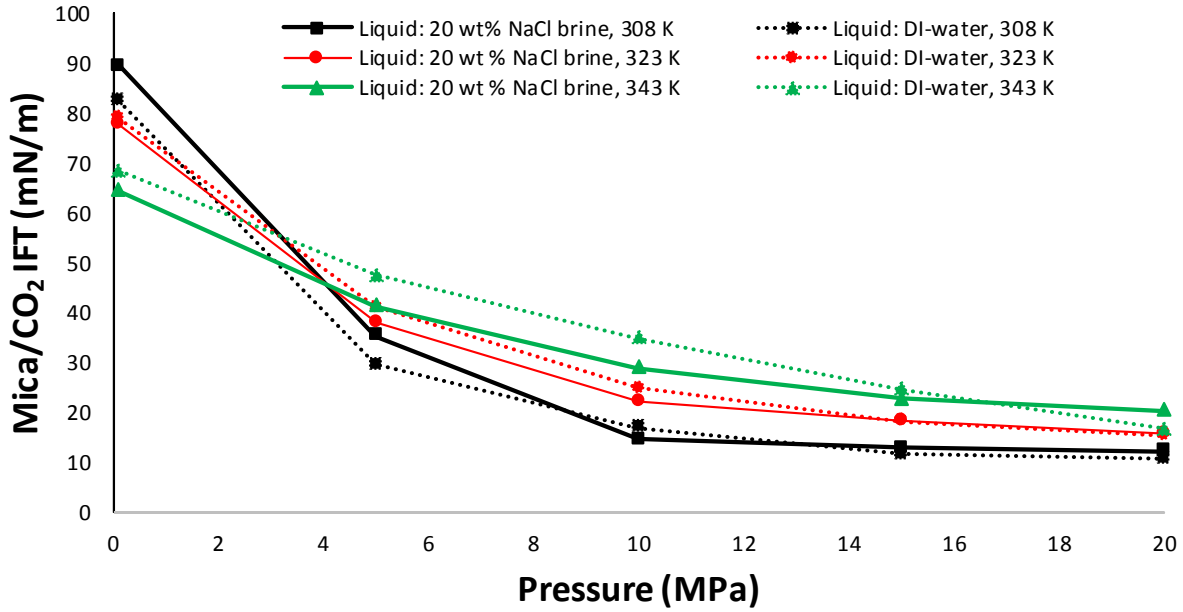

Figure 7: Mica/CO_2 interfacial tension as a function of pressure and temperature for two different liquids (DI-water and 20 wt% NaCl brine)

3.5. Effect of salinity on solid/water interfacial tension

To analyse the effect of salinity on the solid-water interfacial energies, we compared γ_{sw} results for DI water (see above) with that of 20 wt% NaCl brine. The β values from the non-linear regression fit of cosine of the equilibrium contact angle data were 0.000267, 0.000284, and 0.00034 at 308 K, 323 K and 343 K, respectively. The Pearson coefficients were 0.846, 0.921 and 0.941, indicating good fits. The mica/brine (20wt% NaCl) interfacial tensions were 10.5 mN/m, 6.27 mN/m and 4.4 mN/m at 308 K, 323 K and 343 K, respectively implying that mica/brine interfacial tension decreased with temperature, consistent with the solid/DI-water system (discussed above). However, at any given temperature, mica/brine interfacial tension was larger than the mica/water interfacial tension. For instance, at 308 K, mica/brine (20 wt % NaCl brine) interfacial tension was 10.5 mN/m in comparison to 2.1 mN/m for mica/DI water at the same temperature (308 K). This result is consistent with Ameri et al. (2013) who found that when salinity increased from 0wt% NaCl to 3.5 wt% NaCl, γ_{sw} increased slightly. However, Shoaji Kaveh et al. (2016) found a slight reduction in γ_{sw} with salinity. The increase

in solid/brine interfacial tension with salinity is related to the intermolecular forces and the zeta potential which arises due to charged species on the surface. As salinity increases, more counter ions are available to reduce the net charge and thus reduces the polarity of the surface, which again leads to a reduction in water-surface van der Waals forces. Lower van der Waals interactions result in higher interfacial tensions. Moreover, Roshan et al. (2016), recently introduced a model to describe the physical processes for wettability variation as a function of salinity in which they related electric potential at the mineral surface to the contact angle. Their results showed that as salinity increased the surface became more hydrophobic due to a decrease in the dielectric constant of liquid with salinity.

3.6. Wettability dependence on surface energies

In order to evaluate the net effect of these interfacial tensions on contact angle, the right hand side (RHS) of Young's equation (the value of cosθ) was calculated for all cases analysed using the computed values of γ_{sc} , γ_{sw} and experimental values of γ_{cw}. For quartz, cosθ decreases with pressure and temperature because quartz/CO_2 interfacial tension decreases with pressure and increases with temperature, and the quartz/water interfacial tension increases with temperature. Thus the net effect of the three interfacial tension results in decrease in a cosθ with pressure and temperature and consequently θ increases with pressure and temperature for quartz (consistent with experimental data, Table 1). For all other cases (mica and coals), cosθ decreases with pressure and increases with temperature because solid/CO_2 interfacial tension decreases with pressure and increases with temperature and the solid/water interfacial tension also decreases with temperature (for mica and coals), thus θ increases with pressure and decreases with temperature (consistent with experimental data, Table 1).

Moreover, for water-wet mica, cosθ stays positive for all tested pressures and temperatures, because the mica surface remains either strongly water-wet or weakly water-wet (contact angle < 90°, cp. Iglauer et al., 2015a, Table 1); however for the oil-wet mica surface, cosθ reaches negative values for a wide range of tested pressures and temperatures which indicates CO_2-wet conditions exhibited by this surface (contact angle > 90°, Iglauer et al., 2015a, Table 1). Moreover, θ increased more rapidly for oil-wet mica (as compared to water-wet mica), because of the low CO_2-solid interfacial energy, which promotes de-wetting of the surface by water (Dickson et al., 2006). Because high energy fluids (e.g. water), do not tend to spread on low-energy surfaces, the presence of a low energy CO_2 layer will cause the solid/water contact angle to increase above 90° to increase the interfacial area between water and CO_2. Furthermore, for

mica and coals, θ decreases with temperature because the net effect of solid/fluid and fluid/fluid interfacial tensions gives rise to an increase in the cosθ with temperature.

In summary, the increase in contact angle with pressure is due to a reduction in the difference of solid and CO_2 cohesive energies with pressure which leads to more favourable interactions between solid and CO_2. Consequently, γ_{sc} decreases with pressure and thus promotes de-wetting of the surface (i.e. higher water contact angle).

4. Implications

We predicted solid/CO_2 and solid/water interfacial tensions for various rock forming minerals including quartz, mica and coals for a wide range of pressure and temperature conditions. The results imply that the surfaces which are more non-wetting to water exhibit lower values of solid/CO_2 interfacial tension than the surfaces which are more water-wet (e.g. 18 mN/m for water-wet mica in comparison to ~3mN/m for oil-wet mica at 15 MPa and 323 K). Moreover, the less water-wet surfaces have higher solid/water interfacial tensions than the water-wet surfaces (24.8 mN/m for oil-wet mica and ~2 mN/m for water-wet mica, Figure 5). Computations of these surface energies in conjunction with Young Laplace's equation enables us to predict contact angles. As an example, θ values are predicted using Young's equation (Equation 1) using the calculated values of the interfacial tensions and the results are shown at 343 K for all samples analysed (Figure 8). The results show a good match between experimental contact angle and the predicted contact angles. This implies that the methodology considered in this work to compute surface energies is correct and that the predicted solid-fluid interfacial tensions correctly reproduced experimental contact angle data.

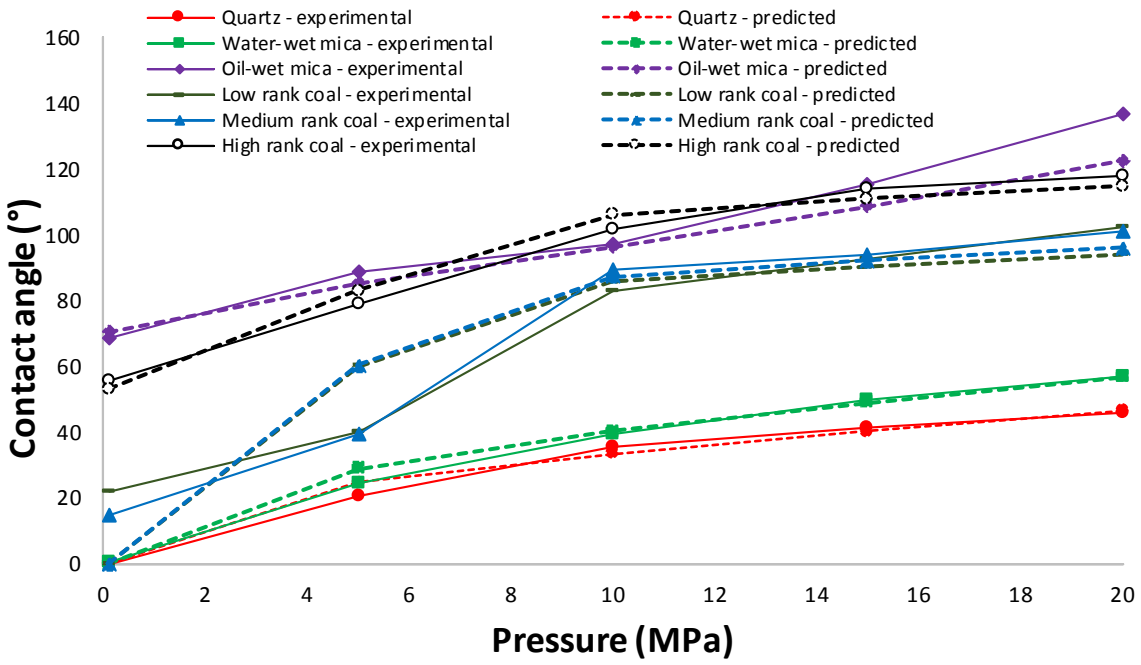

Figure 8: Experimental and predicted water contact angles as a function of pressure at 343 K for all substrates.

In terms of a broader interpretation, the solid/fluid interfacial tensions reported in this study are useful for relating CO_2 storage potential to rock/fluid interfacial tension. For instance, water-wet rocks are better for CO_2 storage (Iglauer et al., 2011) because of higher solid/CO_2 (solid = rock in this case) interfacial tension and oil-wet rocks exhibit poor CO_2-storage potential in terms of structural and residual trapping (Iglauer et al., 2016) due to lower solid/CO_2 interfacial tension (e.g. pure quartz have higher solid/CO_2 interfacial tension than 37%SiOH quartz, section 3.1). Physically, due to higher solid/CO_2 interfacial tension for water-wet rocks, CO_2 tends to stick to the rock (rock offers more resistance to the flow/leakage of buoyant CO_2) and CO_2 is thus rendered immobile within the pores (leading to higher capillary/residual trapping in water-wet rocks; Iglauer et al., 2011). However, the detailed investigation of trapping potential must also account for solubility of CO_2 in the oil phase, sealing tendency of the caprock, and the pore geometry etc. to device suitable field scale storage plans.

5. Conclusions

We used Neumann's equation of state (Neumann et al., 1974) to compute the interfacial tensions of mineral/CO_2 and mineral/water systems for important rock forming minerals (quartz, water-wet mica and oil-wet mica) and for coals of high to low rank as a function of pressure, temperature and salinity. It was found that mineral/CO_2 interfacial tension decreased with pressure (consistent with Ameri et al. 2013 and Dickson et al. 2006), which is due to increased CO_2-mineral intermolecular interactions (e.g. Iglauer et al., 2012, Al-Yaseri et al. 2016b). It was also found that mineral/CO_2 interfacial tensions increased with temperature which is due to an increase in the difference of solid/CO_2 cohesive energies with temperature which thus leads to less favourable interactions between solid and CO_2 (thus higher γ_{sc}). Moreover, the more non-wetting to water the surface was, the lower were the mineral/CO_2 interfacial tensions and the higher were the mineral/water interfacial tensions, e.g. oil-wet mica showed a lower mica/CO_2 interfacial tension than water-wet mica at the same pressure and temperature. Similarly, high rank coal had a lower coal/CO_2 interfacial tension than the low rank coal, because of greater hydrophobicity of high rank coal. This behaviour is attributed to fewer hydrophilic sites in high rank coal as opposed to abundance of hydrophilic sites in low rank coal (confirmed by IR spectroscopy). For all systems, solid/water interfacial tension decreased with temperature, except for quartz, where the quartz/water interfacial tension increased with temperature. The effect of salinity was also analysed and it was found that solid/water interfacial tension increased with salinity. Moreover, contact angles were predicted by Young's equation using the computed values of interfacial energies, and the predicted θ values were in good agreement with the experimental θ values.

We conclude that the Neumann equation of state is adequate to quantify the solid surface energy and that the results demonstrated significant influence of surface energy in controlling the wettability dependence on pressure, temperature and salinity.

References

Al-Yaseri, A. Z., Lebedev, M., Barifcani, A., & Iglauer, S. (2016a). Receding and advancing (CO_2+ brine+ quartz) contact angles as a function of pressure, temperature, surface roughness, salt type and salinity. The Journal of Chemical Thermodynamics, 93, 416-423.

621 Al-Yaseri, A. Z., Roshan, H., Lebedev, M., Barifcani, A., & Iglauer, S. (2016b).
622 Dependence of quartz wettability on fluid density. Geophysical Research Letters, 43(8),
623 3771-3776.

624 Ameri, A., Kaveh, N. S., Rudolph, E. S. J., Wolf, K. H., Farajzadeh, R., & Bruining, J.
625 (2013). Investigation on Interfacial Interactions among Crude Oil–Brine–Sandstone Rock–
626 CO_2 by Contact Angle Measurements. Energy & Fuels, 27(2), 1015-1025.

627 Arif, M., Al-Yaseri, A. Z., Barifcani, A., Lebedev, M., & Iglauer, S. (2016a). Impact of
628 pressure and temperature on CO_2–brine–mica contact angles and CO_2–brine interfacial
629 tension: Implications for carbon geo-sequestration. Journal of Colloid and Interface
630 Science, 462, 208-215.

631 Arif, M., Barifcani, A., Lebedev, M., & Iglauer, S. (2016b). Structural trapping capacity of
632 oil-wet caprock as a function of pressure, temperature and salinity. International Journal of
633 Greenhouse Gas Control, 50, 112-120.

634 Arif, M., Barifcani, A., Lebedev, M., & Iglauer, S. (2016c). CO_2-wettability of low to high
635 rank coal seams: Implications for carbon sequestration and enhanced methane recovery.
636 Fuel, 181, 680-689.

637 Barton, A. F. (1991). CRC handbook of solubility parameters and other cohesion
638 parameters. CRC press.

639 Blunt, M., Fayers, F. J., & Orr, F. M. (1993). Carbon dioxide in enhanced oil recovery.
640 Energy Conversion and Management, 34(9), 1197-1204.

641 Broseta, D., Tonnet, N., & Shah, V. (2012). Are rocks still water-wet in the presence of
642 dense CO2 or H2S? Geofluids, 12(4), 280-294.

643 Brown, M. A., Huthwelker, T., Beloqui Redondo, A., Janousch, M., Faubel, M., Arrell, C.
644 A., ... & van Bokhoven, J. A. (2012). Changes in the silanol protonation state measured in
645 situ at the silica–aqueous interface. The Journal of Physical Chemistry Letters, 3(2), 231-
646 235.

647 Bustin, R. M., & Clarkson, C. R. (1998). Geological controls on coalbed methane reservoir
648 capacity and gas content. International Journal of Coal Geology, 38(1), 3-26.

649 Chen, C., Wan, J., Li, W., & Song, Y. (2015). Water contact angles on quartz surfaces
650 under supercritical CO 2 sequestration conditions: Experimental and molecular dynamics
651 simulation studies. International Journal of Greenhouse Gas Control, 42, 655-665.

652 Chiquet, P., Broseta, D., & Thibeau, S. (2007). Wettability alteration of caprock minerals
653 by carbon dioxide. Geofluids, 7(2), 112-122.
654 Dickson, J. L., Gupta, G., Horozov, T. S., Binks, B. P., & Johnston, K. P. (2006). Wetting
655 phenomena at the CO_2/water/glass interface. Langmuir, 22(5), 2161-2170.
656 El-Maghraby, R. M., Pentland, C. H., Iglauer, S., & Blunt, M. J. (2012). A fast method to
657 equilibrate carbon dioxide with brine at high pressure and elevated temperature including
658 solubility measurements. The Journal of Supercritical Fluids, 62, 55-59.
659 Fowkes, F. M. (1964). Attractive forces at interfaces. Industrial & Engineering Chemistry,
660 56(12), 40-52.
661 Fox, H. W., & Zisman, W. A. (1952). The spreading of liquids on low-energy surfaces. III.
662 Hydrocarbon surfaces. Journal of colloid science, 7(4), 428-442.
663 Iglauer, S., Paluszny, A., Pentland, C. H., & Blunt, M. J. (2011). Residual CO2 imaged
664 with X-ray micro-tomography. Geophysical Research Letters, 38(21).
665 Iglauer, S., Mathew, M. S., & Bresme, F. (2012). Molecular dynamics computations of
666 brine–CO_2 interfacial tensions and brine–CO_2–quartz contact angles and their effects on
667 structural and residual trapping mechanisms in carbon geo-sequestration. Journal of colloid
668 and interface science, 386(1), 405-414.
669 Iglauer, S., Paluszny, A., & Blunt, M. J. (2013). Simultaneous oil recovery and residual gas
670 storage: A pore-level analysis using in situ X-ray micro tomography. Fuel, 103, 905-914.
671 Iglauer, S., Pentland, C. H., & Busch, A. (2015a). CO_2 wettability of seal and reservoir
672 rocks and the implications for carbon geo-sequestration. Water Resources Research, 51(1),
673 729-774.
674 Iglauer, S., Al-Yaseri, A. Z., Rezaee, R., & Lebedev, M. (2015b). CO2 wettability of
675 caprocks: Implications for structural storage capacity and containment security.
676 Geophysical Research Letters, 42(21), 9279-9284.
677 Iglauer, S., Rahman, T., Sarmadivaleh, M., Al-Hinai, A., Fernø, M. A., & Lebedev, M.
678 (2016). Influence of Wettability on Residual Gas Trapping and Enhanced Oil Recovery in
679 Three-Phase Flow: A Pore-Scale Analysis by Use of Microcomputed Tomography. SPE
680 Journal.
681 IPCC, Working Group III of the Intergovernmental Panel on Climate Change, vol. 1, 2005,
682 p. 443.

683 Janczuk, B., & Zdziennicka, A. (1994). A study on the components of surface free energy
684 of quartz from contact angle measurements. Journal of materials science, 29(13), 3559-
685 3564.
686 Javanbakht, G., Sedghi, M., Welch, W., & Goual, L. (2015). Molecular Dynamics
687 Simulations of CO2/Water/Quartz Interfacial Properties: Impact of CO2 Dissolution in
688 Water. Langmuir, 31(21), 5812-5819.
689 Kittel, C. (2005). Introduction to solid state physics. Wiley.
690 Krevor, S., Pini, R., Zuo, L., & Benson, S. M. (2012). Relative permeability and trapping
691 of CO2 and water in sandstone rocks at reservoir conditions. Water Resources Research,
692 48(2).
693 Krevor, S., Blunt, M. J., Benson, S. M., Pentland, C. H., Reynolds, C., Al-Menhali, A., &
694 Niu, B. (2015). Capillary trapping for geologic carbon dioxide storage–From pore scale
695 physics to field scale implications. International Journal of Greenhouse Gas Control, 40,
696 221-237.
697 Kwok, D. Y., & Neumann, A. W. (1999). Contact angle measurement and contact angle
698 interpretation. Advances in colloid and interface science, 81(3), 167-249.
699 Kwok, D. Y., & Neumann, A. W. (2000). Contact angle interpretation in terms of solid
700 surface tension. Colloids and Surfaces A: Physicochemical and Engineering Aspects,
701 161(1), 31-48.
702 Lackner, K. S. (2003). A guide to CO2 sequestration. Science, 300(5626), 1677.
703 Li, D., & Neumann, A. W. (1992). Equation of state for interfacial tensions of solid-liquid
704 systems. Advances in Colloid and Interface Science, 39, 299-345.
705 Li, X., Boek, E., Maitland, G. C., & Trusler, J. M. (2012a). Interfacial Tension of (Brines+
706 CO_2) :(0.864 NaCl+ 0.136 KCl) at Temperatures between (298 and 448) K, Pressures
707 between (2 and 50) MPa, and Total Molalities of (1 to 5) mol· kg–1. Journal of Chemical
708 & Engineering Data, 57(4), 1078-1088.
709 Liu, S., Yang, X., & Qin, Y. (2010). Molecular dynamics simulation of wetting behavior
710 at CO2/water/solid interfaces. Chinese Science Bulletin, 55(21), 2252-2257.
711 Lun, Z., Fan, H., Wang, H., Luo, M., Pan, W., & Wang, R. (2012). Interfacial Tensions
712 between Reservoir Brine and CO_2 at High Pressures for Different Salinity. Energy & Fuels,
713 26(6), 3958-3962.
714 Manoj, B., Kunjomana, A. G., & Chandrasekharan, K. A. (2009). Chemical leaching of
715 low rank coal and its characterization using SEM/EDAX and FTIR. Journal of Minerals
716 and Materials Characterization and Engineering, 8(10), 821.

McCaughan, J., Iglauer, S., & Bresme, F. (2013). Molecular dynamics simulation of water/CO 2-quartz interfacial properties: application to subsurface gas injection. Energy Procedia, 37, 5387-5402.

Neumann, A. W., Good, R. J., Hope, C. J., & Sejpal, M. (1974). An equation-of-state approach to determine surface tensions of low-energy solids from contact angles. Journal of Colloid and Interface Science, 49(2), 291-304.

Owens, D. K., & Wendt, R. C. (1969). Estimation of the surface free energy of polymers. Journal of applied polymer science, 13(8), 1741-1747.

Roshan, H., Al-Yaseri, A. Z., Sarmadivaleh, M., & Iglauer, S. (2016). On wettability of shale rocks. Journal of colloid and interface science, 475, 104-111.

Saraji, S., Piri, M., & Goual, L. (2014). The effects of SO2 contamination, brine salinity, pressure, and temperature on dynamic contact angles and interfacial tension of supercritical CO2/brine/quartz systems. International Journal of Greenhouse Gas Control, 28, 147-155.

Sarmadivaleh, M., Al-Yaseri, A. Z., & Iglauer, S. (2015). Influence of temperature and pressure on quartz–water–CO_2 contact angle and CO_2–water interfacial tension. Journal of colloid and interface science, 441, 59-64.

Sarwar, A., Khan, M. N., & Azhar, K. F. (2012). Coal chemistry and morphology of thar reserves, Pakistan. Journal of Minerals and Materials Characterization and Engineering, 11(08), 817.

Schaeff, H. T., & McGrail, B. P. (2004). Direct measurements of pH in H2O-CO2 brine mixtures to supercritical conditions. In Proceedings of the 7th International Conference on Greenhouse Gas Control Technologies (GHGT-7).

Shojai Kaveh, N. S., Wolf, K. H., Ashrafizadeh, S. N., & Rudolph, E. S. J. (2012). Effect of coal petrology and pressure on wetting properties of wet coal for CO2 and flue gas storage. International Journal of Greenhouse Gas Control, 11, S91-S101.

Shojai Kaveh, N., Barnhoorn, A., & Wolf, K. H. (2016). Wettability evaluation of silty shale caprocks for CO_2 storage. International Journal of Greenhouse Gas Control, 49, 425-435.

Socrates, G. (2004). Infrared and Raman characteristic group frequencies: tables and charts. John Wiley & Sons.

Staszczuk, P. (1989). On the determination of surface free energy of coal by means of the derivatograph. Fuel science & technology international, 7(1), 89-101.

749 Siemons, N., Bruining, H., Castelijns, H., & Wolf, K. H. (2006). Pressure dependence of
750 the contact angle in a CO2–H2O–coal system. Journal of Colloid and Interface Science,
751 297(2), 755-761.
752 Tadmor, R. (2004). Line energy and the relation between advancing, receding, and young
753 contact angles. Langmuir, 20(18), 7659-7664.
754 Tripp, C. P., & Combes, J. R. (1998). Chemical modification of metal oxide surfaces in
755 supercritical CO2: The interaction of supercritical CO2 with the adsorbed water layer and
756 the surface hydroxyl groups of a silica surface. Langmuir, 14(26), 7348-7352.
757 Van Oss, C. J., Good, R. J., & Chaudhury, M. K. (1986). The role of van der Waals forces
758 and hydrogen bonds in "hydrophobic interactions" between biopolymers and low energy
759 surfaces. Journal of colloid and Interface Science, 111(2), 378-390.
760 Wu, S. (1971, January). Calculation of interfacial tension in polymer systems. In Journal
761 of Polymer Science Part C: Polymer Symposia (Vol. 34, No. 1, pp. 19-30). Wiley
762 Subscription Services, Inc., A Wiley Company.
763 Wu, D., Liu, G., & Sun, R. (2014). Investigation on structural and thermodynamic
764 characteristics of perhydrous bituminous coal by fourier transform infrared spectroscopy
765 and thermogravimetry/mass spectrometry. Energy & Fuels, 28(5), 3024-3035.
766 Żenkiewicz, M. (2007). Methods for the calculation of surface free energy of solids. Journal
767 of Achievements in Materials and Manufacturing Engineering, 24(1), 137-145.